Arch. Mech., **54**, 2, pp. 155–174, Warszawa 2002

Experimental study of a PA66 solid polymer in the case of cyclic shear loading

G. BLES[1], S.P. GADAJ[2], W.K. NOWACKI[2], A. TOURABI[1]

(1) *Laboratoire Sols Solides Structures, Domaine Universitaire, B.P. n° 53, 38041 Grenoble cedex 9, France*

(2) *Center of Mechanics and Information Technology, Institute of Fundamental Technological Research, Polish Academy of Sciences, Świętokrzyska 21, 00-049 Warsaw, Poland*

EXPERIMENTAL MECHANICAL RESULTS concerning cyclic shear tests without lateral force and simple shear tests with measurement of temperature, performed on sheet samples of PA66 polyamide, are presented. These tests are performed using special shear devices, attached to a classical tensile testing machine. The aim of our work was the examination of thermomechanical characteristics of solid polyamide during shear loading. This study allowed us to analyse the changes of the stress and strain characteristics, shear modulus, ratcheting, relaxation effects and thermomechanical effects.

1. Introduction

SINCE THE BEGINNING of the twentieth century, it is an established fact that the mechanical behaviour of solid materials under rotational loading shows second-order effects [1,2]. Thus, during torsion of a wire, a bar or a tube, we measure the variation in the axial strain if the axial load is kept equal to zero [3], and a variation in the axial load if the axial strain is kept equal to zero [4]. When the rotational loading is cyclic, these effects accumulate and show a phenomenon of ratchet [5]. The experimental study of this phenomenon gives essential information to make theoretical choices about the second-order tensorial coupling effects of the ratchet type. These effects are very sensitive to the definition of Preferred Reference Frames spins [6,7]. The present work is a preliminary study in order to find the generic parts of the thermomechanical behaviour of the PA66 polyamide during the rotational loading of shear.

Two types of shear devices were used. The first one allows the shear tests without lateral force in order to characterise the mechanical behaviour during cyclic shear tests, relaxation and creep tests. The first and the second-order effects were observed. The second device performs a simple shear test with

a measurement of temperature. An infrared thermovision camera was used. The thermomechanical effects were observed.

This paper presents at first the experimental facilities used; we explain the principle of the shear devices with which a classical tensile machine can make the shear test. The material and the shear samples are presented. A local strain measure was done in a homogeneous area of the sample. Secondly, we present the results of these tests. During symmetric cyclic shear tests with several amplitudes, the shear stress and strain were observed. Then, the evolution of the second-order effects or ratchet during these cyclic shear tests is presented. Tests with relaxations and creeps show specific evolution of the first and second-order effects. During the simple shear tests, thermomechanical coupling was examined.

2. Experimental facilities and methods

2.1. Shear device without lateral force

The cyclic shear is obtained using a device allowing to change the tension-compression mode of loading into cyclic shear mode of loading [9]. This shear device is essentially composed of a very rigid frame consisting of a rectangular box, inside which vertical and a horizontal carriages move (Fig.1). The device is attached to a classical tensile testing machine by means of a fixed and a moving grip. The horizontal carriage is capable of performing vertical and horizontal translations, in the plane of shear. The sample is connected to the apparatus, between the frame and the horizontal carriage, by two clamping devices.

The vertical translation of the moving grip imposes the shear motion on the sample; the horizontal translation is free of load and allows a shear with no lateral force, like the simple torsion test tube without axial force [10]. These two translations are obtained using two pairs of linear guides located symmetrically with respect to the horizontal and vertical carriages. To obtain a shear test as correct as possible, we control the mechanical clearance for each pair of linear guides by using two adjustable looseness devices. The aim of this adjustment is an ideal situation of motion without friction and slack. This adjustable looseness device avoids an excessive friction, which hampers the shear test and its measurement. This device avoids mechanical clearances too, which are not convenient for the shear test while the machine load is changing from tension to compression. The shear device is fitted on the testing machine with a counterweight. Thus, in addition to the mobility of the horizontal carriage, it is possible to clamp the sample without any stress. Moreover, the dimensions of the shear device were overestimated toward the effective loading, in order to get a high stiffness for an allowed shear force of 25 KN [9].

The principle of this present device differs from other shear devices [11,12] because it can perform a shear in which the lateral load is equal to zero. During the shear, the horizontal carriage movement free of load makes the lateral strain ratchet possible. The measure of this displacement during cyclic shear gives interesting information. Using this device, the characterisation of material's behaviour is more precise owing to the measure of both the main and the second-order effects.

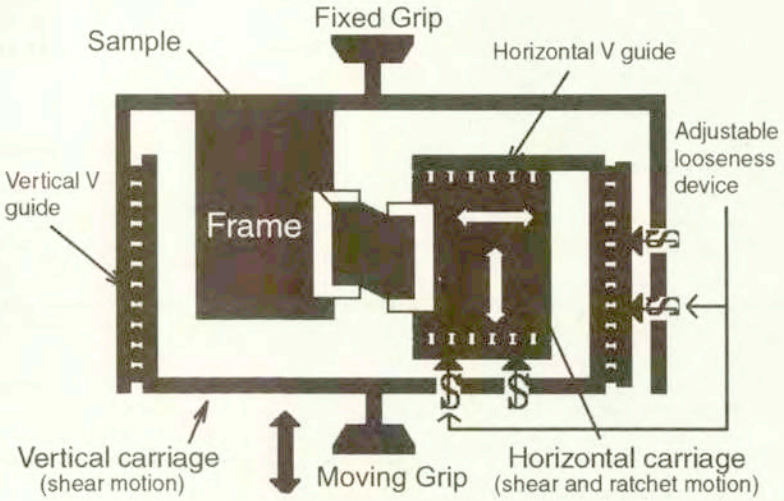

FIG. 1. Principle of the shear device without lateral force.

2.2. Simple shear device with measurement of temperature

The simple shear was made in a specially designed grip, transforming the compression into a simple plain shear. Construction of this arrangement practically eliminates sliding of the specimen in the grip and ensures that the process of shear takes place on two parallel shear bands of the specimen [13]. This grip was fitted in the testing machine.

During the deformation, the load, displacement and the distribution of infrared radiation emitted by shear paths are continuously registered. The infrared radiation is measured using the thermovision camera [13].

The distribution of intensity of the infrared radiation, recorded during investigation in a digital form, allows us to reconstruct thermal pictures (thermograms) of the specimens. In Fig. 2, an example of a thermogram of the shear zones of the deformed specimen is shown.

After measurement on each of the sheared paths of the thermogram, the central line along the shear direction is drawn (Fig. 2). The temperature changes are found as average values of the temperature along these lines.

The mean-square error of temperature evaluation, obtained in this way, is 0,2 / 0,3 K.

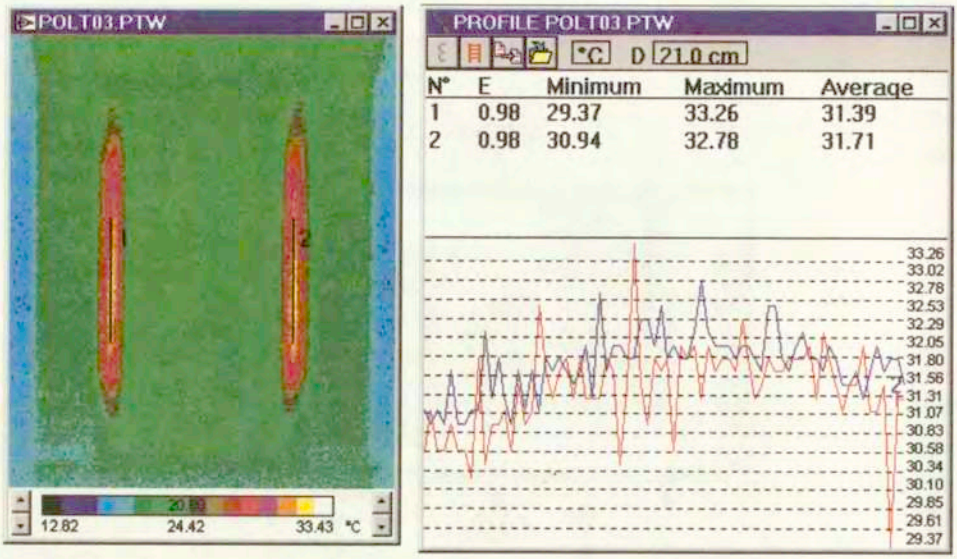

FIG. 2. Example of a thermogram obtained during simple shear tests.

2.3. Edge effects

The shear test has several advantages from the fundamental point of view and the experimental point of view. Nevertheless, it has a disadvantage because of its principle; the shear stress field is heterogeneous along the shear band. Actually, the shear stress is constant inside the $\alpha\beta\chi\delta$ zone in the middle of the sample (Fig. 3a), but it vanishes at the two free ends of the sample at points A, B, C and D. The equilibrium of this $\alpha\beta\chi\delta$ element, in the sheared zone, requires that shear stresses on perpendicular faces should be equal in magnitude and have directions such that the resulting moment acting on the element is balanced. This property is the result of Cauchy's principle of reciprocity of shear stress. On the edges AB and CD, the stress at these sides is equal to zero. So, the shear stress field is not homogeneous in the αABβ and χCDδ zones, near the ends of the sample. In order to reduce the effect of the edge heterogeneity, we choose usually the shear band height greater than ten times its width: $H/B > 10$ [13, 14].

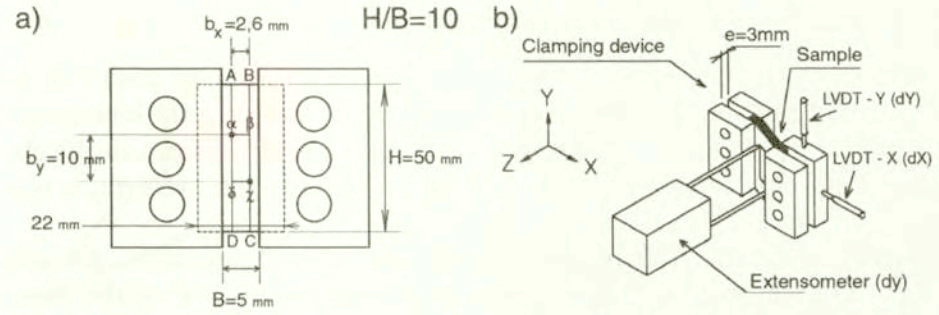

FIG. 3. (a) dimensions of the shear sample clamped, (b) global and local measures of the two shear strains.

2.4. Studied material and shear samples

The material is the polyamide PA66, that is a semicrystalline thermoplastic polymer. Differential Scanning Calorimetry (DSC) method gives the glass transition temperature T_g, the melting temperature T_m and the percentage of crystallinity C. Supposing a normal distribution, we determine the mean value $<x>$ of T_g, T_m and C as well as the standard deviation σ_x of the n individual values distribution, and $\sigma_{<x>}$ of the mean value distribution (Table 1).

Table 1. Glass transition, melting temperatures and percentage of crystallinity of sample's material (PA66).

Measure	$< x >$	$+/- 2\ \sigma_{<x>}$
T_g	51.8 °C	+/- 1.9 °C
T_m	263.6 °C	+/- 1.7 °C
C	34.7 %	+/- 3.5 %

The investigations were performed on PA66 sheet samples. Thickness e of these samples is 3 mm. The overall dimensions of the samples used with the shear device without lateral force are 50 mm x 22 mm x 3 mm (Fig. 3). The dimensions of the samples used with the simple shear device are 30 mm x 42,3 mm x 3 mm. The dimensions of the shear band in the two cases are :

- shear device without lateral force; $H = 50$ mm, $B = 5$ mm, $e = 3$ mm,
- simple shear device; $H = 30$ mm, $B = 3$ mm, $e = 3$ mm.

Then two conditions for the shear tests are satisfied [1]:

- the ratio of B to e (B/e=1,66 and B/e=1) is small enough to avoid buckling of the sheared zone,
- the ratio of H to B (H/B=10) is great enough to minimise the error due to non-homogeneity of the shear stress and strain at the two free ends.

2.5. Principles of stress and strain measurements

Assuming that there is no change in the cross section of shear path [3], and assuming that the ratio H/B equal to 10 is sufficient concerning the homogeneity of stress field, we can obtain the stress σ_{xy} as the ratio of the force to the cross section. In the case of a shear device without lateral force, the stress σ_{xx} is equal to zero.

During the simple shear tests with measurement of temperature, the strain ε_{xy} was obtained classically from the relative displacement dY of the clamps and the width B of the shear band:

$$\varepsilon_{xy} = dY/2B. \tag{2.1}$$

During the shear tests without lateral force, values ε^g_{xy} and ε^g_{xx} of the strains ε_{xy} and ε_{xx} were obtained from the relative displacement of the clamps, dX and dY (Fig. 3b). These measures are called global, as opposed to the local strain measure performed by means of an extensometer (Fig. 3b) in an area in the middle of the shear sample. ε^g_{xy} and ε^g_{xx} were not calculated classically using the width of the shear band, but with a corrected value of this width, called B_g:

$$\varepsilon^g_{xy} = dY/2B_g, \quad \varepsilon^g_{xx} = dX/B_g. \tag{2.2}$$

This value B_g was obtained by comparison (Fig. 4c) of the measure Y and a measure ε_{xy} realised locally by the extensometer (Fig. 3b) ; $B_g = 6{,}49$ mm. This value is greater than the width of the shear band $B = 5$ mm; in fact, a small slide of the sample inside the clamps occured as it was observed on the clamp impression on the sample, which is bell-shaped over a distance of 1 mm from the clamp edge; $B + 1$ mm $+ 1$ mm $= 7$ mm $\sim B_g$.

A special extensometer allowed us to measure the shear strain ε_{xy} in a local area in the middle of the sample; the $\alpha\beta\chi\delta$ rectangle in the Fig. 3a. Assuming the strain homogeneity in this reference rectangle, this value ε_{xy} was obtained from the relative displacement dy (Fig. 3b), given by the extensometer, and the initial width b_x (Fig. 3a) of the $\alpha\beta\chi\delta$ area:

$$\varepsilon_{xy} = dy/2b_x. \tag{2.3}$$

The necessity of local strain measurement is fully justified in the case of metallic materials (Fig. 4b) [9]. We can compare the measure Y of relative displacement of the clamps and the local strain measure ε_{xy} in the Fig. 4d; a large hysteresis loop appears in the Y-ε_{xy} graph. In the case of PA66 polyamide, the thickness of the loop is smaller. It indicates that clamping of the polyamide sample is more efficient and the sliding zone under the clamps is smaller than that in the case of metallic samples.

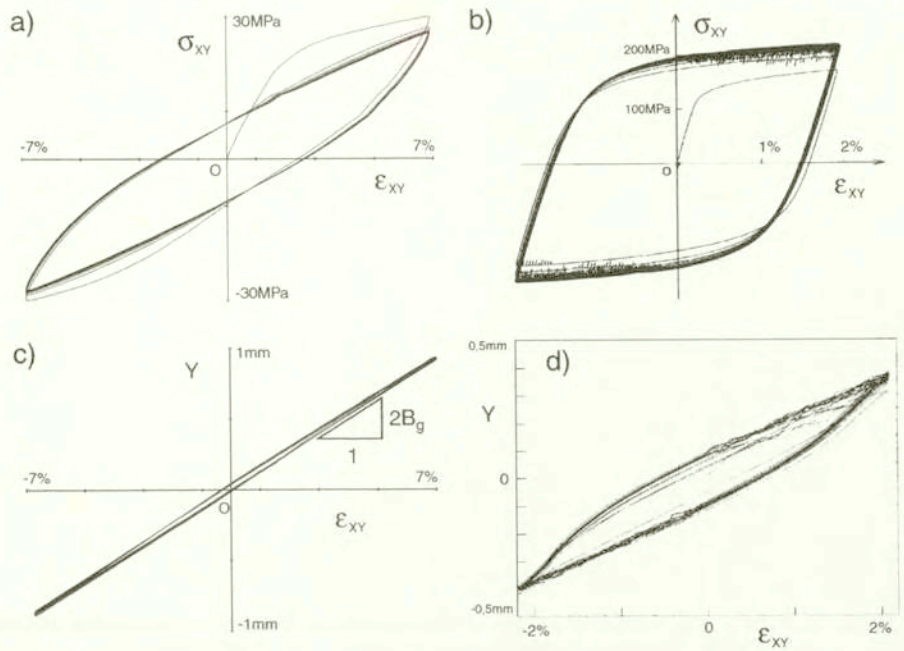

FIG. 4. (a,c) cyclic shear of a polyamide PA66 sample, (b,d) cyclic shear of a metallic sample [9].

3. Results and discussion

This section presents first (Secs. 3.1, 3.2, 3.3, and 3.4) the experimental results obtained with the shear device without lateral force. Secondly Sec. 3.5, the thermomechanical results obtained by the simple shear device with measure of temperature are presented.

3.1. Cyclic shear at constant intensity of strain rate

Two kinds of cyclic shear test at constant intensity of strain rate ($\dot{\varepsilon}_{xy} = 1,1.10^{-3}s^{-1}$) were performed; one with decreasing and one with increasing amplitudes of cycles (Fig. 5a and 5b, respectively). Elastic (or highly-elastic) hysteresis-type behaviour with transient hardening effect during the first loading and weak softening during the cyclic path is observed.

The evolution diagram of the shear stress at the reversal points (Fig. 5c) shows that the saturation values seem to be independent of the history of the cycle amplitudes; increasing and decreasing amplitudes of the cycle do not change the stress saturation value of the cyclic softening.

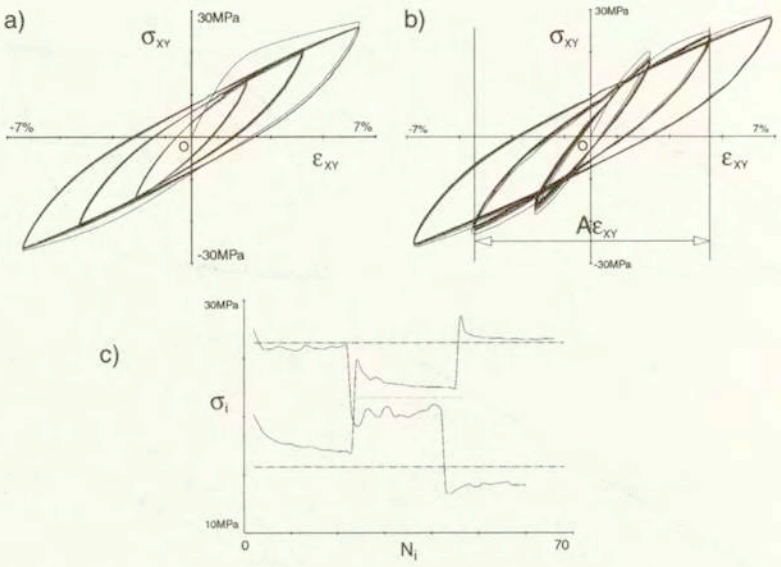

FIG. 5. (a) cyclic shear at decreasing amplitudes and (b) at increasing amplitudes, (c) shear stress at the reversal points during the tests of the Figs. 5a and 5b.

The shear modulus μ was determined by separating the stress-strain curve in loading branches, starting at the origin or at the inversion state (Fig. 6a). The experimental data were transformed in the loading branch space by the co-ordinates (Fig. 6b):

$$\Delta\sigma_{xy} = \sigma_{xy} - {}_R\sigma_{xy}, \quad \Delta\varepsilon_{xy} = \varepsilon_{xy} - {}_R\varepsilon_{xy} \tag{3.1}$$

where: ${}_R\sigma_{xy}$ and ${}_R\varepsilon_{xy}$ were the reference "R_i" co-ordinates of each "i" loading branch. The slope M_μ

$$M_\mu = \frac{1}{2}\left(\frac{d(\Delta\sigma_{xy})}{d(\Delta\varepsilon_{xy})}\right) = \frac{1}{2}\frac{d\sigma_{xy}}{d\varepsilon_{xy}} \tag{3.2}$$

was determined by a spline technique; Fig. 6c.

The shear moduli μ and $\hat{\mu}$ are the slopes at the beginning and at the end of each branch (Fig. 7a):

$$\mu = \lim_{\Delta\varepsilon\to 0} M_\mu, \quad \hat{\mu} = \lim_{\Delta\varepsilon\to\infty} M_\mu \tag{3.3}$$

The distinction between the initial modulus μ and the residual modulus $\hat{\mu}$ evolution during cyclic test is shown in Figs. 7b and 7c. These figures show plainly a transient stage followed by a saturation; according to the modulus μ, the transient stage occurs until the fifth reversal point or during the first two cycles,

whereas the transient stage of the modulus $\hat{\mu}$ is finished at the third reversal point or after the first cycle.

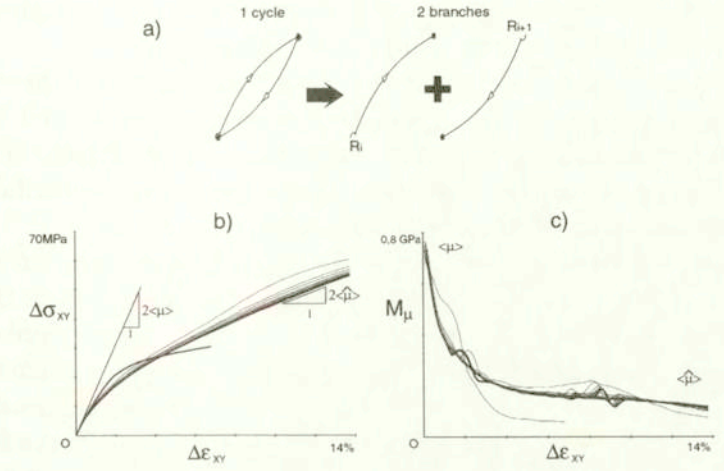

FIG. 6. (a) definition of a branch in a cycle and its reference state "R_i", (b) branches during the cyclic shear test given by the Fig. 4a, (c) shear modulus in the branches at the Fig. 6b.

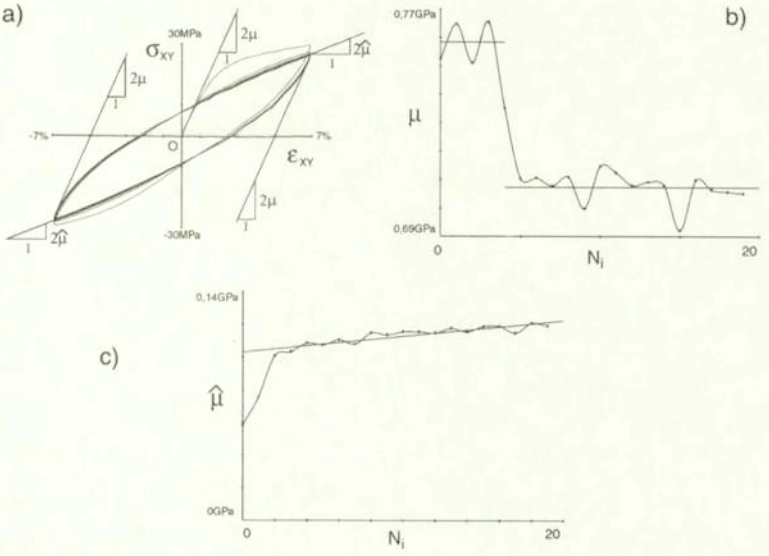

FIG. 7. (a) definition of the shear moduli μ and $\hat{\mu}$, (b) variations of the initial shear modulus μ, (c) variations of the residual shear modulus $\hat{\mu}$.

3.2. Second-order effects

A simple shear with no lateral force leads also to a lateral deformation, which is a lengthening. This is the second-order effect of the shear, comparable to the axial deformation of a torsion test with no axial force [2].

The evolution of lateral deformation versus shear strain for the cyclic tests with decreasing and increasing amplitudes is shown in Figs. 8a and 8b, respectively. This lateral deformation is very small in comparison with the shear strain, but it is not possible to neglect it since this deformation accumulates during cyclic loading and leads to a ratchet phenomenon.

The lateral ratchet evolution can be displayed by the evolution of the lateral strain at the reversal point of each loading branch $\varepsilon_{xx}^{g\,i}$ versus the loading branch number N_i. This is shown in the Fig. 8c for the tests with decreasing and increasing amplitudes of shear cycles. The evolution of the ratcheting effect depends on the order (increasing or decreasing) of the cycle amplitude. But, at the end of these two tests, at about the sixtieth reversal point in the Fig. 8c, the reached ratchet value is the same for these two orders of cycle amplitude. Then, we can say that the ratchet, reached after a series of cyclic tests with different amplitudes, is independent of the order of tests of this series.

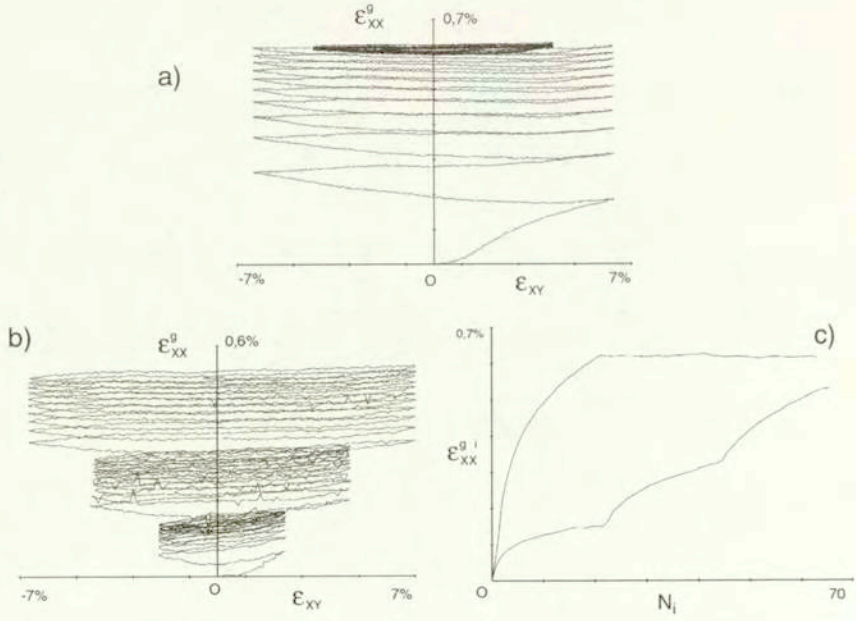

FIG. 8. (a) second-order effect during the shear test with decreasing amplitudes (Fig. 5a), (b) second-order effect during the shear test with increasing amplitudes (Fig. 5b), (c) lateral strain at the reversal point during the shear tests with decreasing and increasing amplitudes.

The ratchet intensity may be characterised by the ratio K of the amount of the ratchet per cycle:

$$K = \Delta\varepsilon^g_{xx}/A\varepsilon_{xy}, \tag{3.4}$$

where $\Delta\varepsilon^g_{xx}$ is the ratchet amplitude per cycle and $A\varepsilon_{xy}$ – the shear strain amplitude of the cycles. For a given shear strain amplitude $A\varepsilon_{xy}$, the ratio K systematically diminishes with the number of cycles, from an initial value $K_{(1)}$ defined in the beginning of cyclic sequence, to a final value $K_{(2)}$ defined at the end of the cyclic sequence. Figure 9a illustrates the variations of the rate of the ratchet $\Delta\varepsilon^g_{xx(1)}$ and $\Delta\varepsilon^g_{xx(2)}$, at the beginning and the end of two cyclic sequences $A\varepsilon^{\mathrm{I}}_{xy}$ and $A\varepsilon^{\mathrm{II}}_{xy}$ $(A\varepsilon^{\mathrm{I}}_{xy} < A\varepsilon^{\mathrm{II}}_{xy})$, which correspond respectively with the definition of the ratios $K_{(1)}$ and $K_{(2)}$, for each of the two amplitudes. In the Fig. 9b are shown changes of the values $K_{(1)}$ and $K_{(2)}$ as a function of $A\varepsilon_{xy}$ obtained for three samples tested with three different shear strain amplitudes, and in the Fig. 9c those obtained for only one sample tested with three increasing amplitudes of cycles. In the first case, the initial value $K_{(1)}$ increases monotonously versus the shear amplitude and the value $K_{(2)}$ is almost in a steady state. In the second one, when the shear strain amplitude increases, using the same sample, we observe a strong decrease in $K_{(1)}$. This result shows the influence of the succession of the cyclic sequences at increasing shear strain amplitudes over the variations of the ratio K, which characterises the amount of the ratchet per cycle.

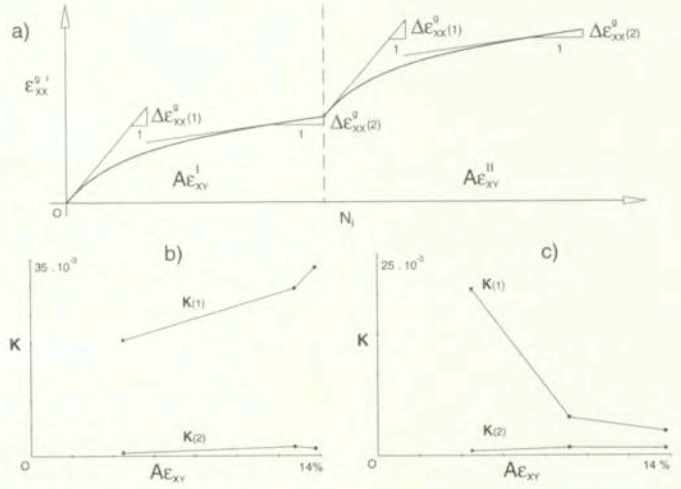

FIG. 9. (a) illustration of the rate of variation of the lateral strain at the beginning and the end of two cyclic sequences $(A\varepsilon^{\mathrm{I}}_{xy} < A\varepsilon^{\mathrm{II}}_{xy})$, (b) rate K of variation of the lateral strain during cyclic shear tests at three amplitudes on three samples, (c) rate K of variation of the lateral strain during one cyclic shear test at three increasing amplitudes on the same sample.

3.3. Relaxation effects

To study the relaxation effects, a strain-controlled test with a constant intensity of strain rate was performed. This test contains two parts:

- In the first one (Fig. 10a), the sample was submitted to a symmetric cyclic loading through ten cycles. During this preliminary cyclic shear, the quasi-stabilised state was reached, what is indicated by stress at the reversal point of cycles (Fig. 10c).
- In the second one (Fig. 10b), only one cycle was performed endowed with relaxation sequences in several points, with the unique duration of 300 seconds. In the $\sigma - \varepsilon$ diagram, the relaxation sequences are pointed by AB, CD, EF, GH and IJ.

A comparison of the $\sigma - \varepsilon$ diagrams of these parts are shown in the Fig. 10d. In first step of the test, we can observe a transient hardening effect during the first cycle loading, and stabilisation in the successive step. During the cycle with the relaxation sequences, the $\sigma - \varepsilon$ hysteresis loop becomes distanced from this stabilised cycle. We observe a hardening phenomenon during this cycle, after the relaxation sequences, very close to the first loading.

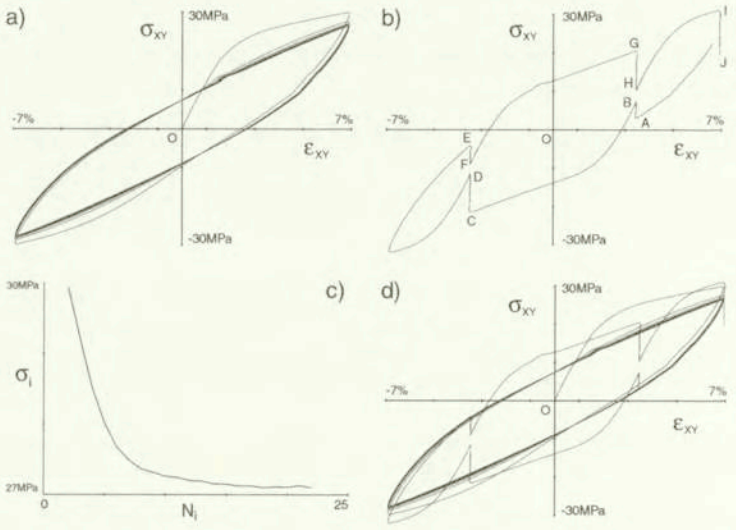

FIG. 10. (a) cyclic symmetric shear test, (b) one cycle with relaxations during 300 seconds, (c) variations of the shear stress at the reversal point during the cyclic shear test (Fig10a), (d) comparison of the cyclic shear test to the cycle with relaxations.

The relaxation effects could be shown from the second-order point of view (Fig. 11). During the first part of the test (ten symmetric cycles), the ratchet evolution is classic (Fig. 11a and 11b). The ratchet intensity increases quickly at

the beginning of the test and seems to tend to a stabilisation value at the end. During the relaxation sequences of the last cycle, a sharp drop in ratchet intensity occurs (Fig. 11c and 11d); and regardless of the position of the relaxation sequence in the cycle.

It should be noted that the drop of the ratchet intensity during relaxation seems to be related to the viscous phenomenon: two ratchet relaxations in the same branch seem, indeed, to have the same saturation threshold (AB and CD or EF and GH in the Fig. 11d).

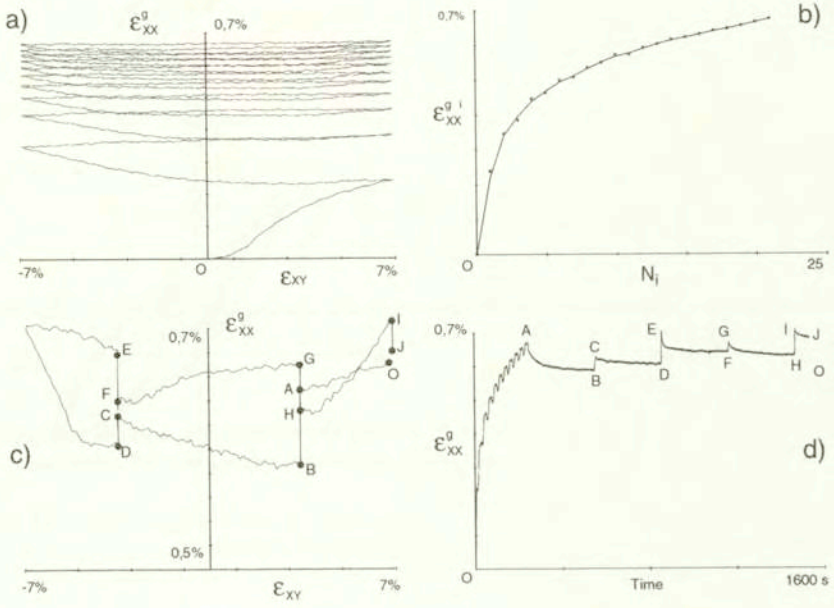

FIG. 11. Second-order effect (a,b) during the cyclic symmetric shear test of the Fig. 10a, and (c,d) during the cycle with relaxations (Fig. 10b).

The stress, during the relaxation sequences, increases or decreases according to the position of the relaxation in the $\sigma - \varepsilon$ hysteresis loop (Fig. 12a). It has a sign opposite to the stress rate in the $\sigma - \varepsilon$ cycle before relaxation.

During relaxation, the variation in stress could be analysed as the evolution of the stress value as a function of time (Fig. 12b). The existence of three main stages is observed: at first, the stress increases and decreases quickly during a few seconds (stage I), in the next (stage II), the evolution of the stress is cut down and we can observe a saturation state in stage III.

To compare the stress and ratchet evolution during relaxation sequence, for example EF, we use a norm by values of stress and lateral strain in the saturation state: $\frac{\varepsilon^g_{xx}}{\varepsilon^{g\,\infty}_{xx}}$ and $\frac{\sigma}{\sigma^\infty}$ (Fig. 12c). Their comparison shows already the connection

between the decrease of ratchet intensity and the stress evolution during the relaxation due to the viscous phenomena.

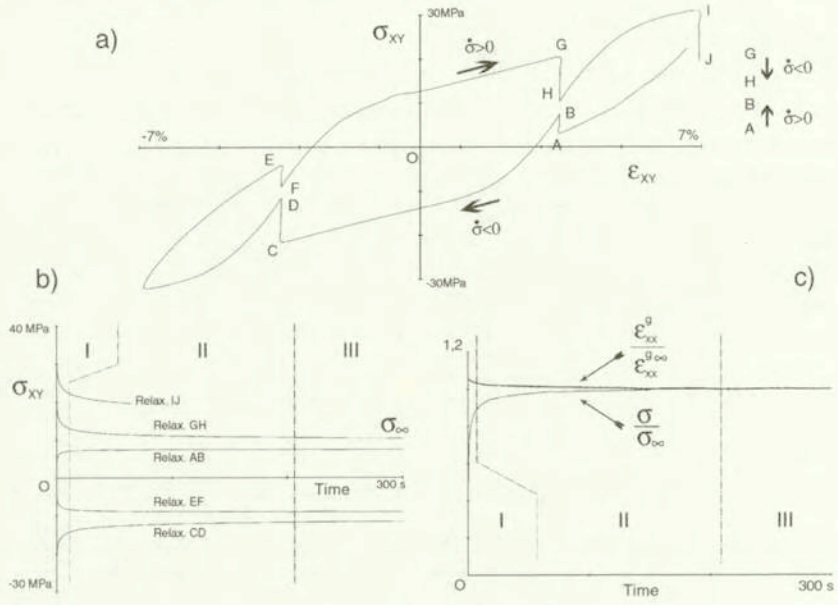

FIG. 12. Variations of the shear stress (a,b) during the relaxations, and (c) comparison of the stress variations to the lateral strain variations during the EF relaxation.

3.4. Creep effects

To observe the creep effects during cyclic shear, a stress-controlled test with a constant intensity of stress rate was performed. This test has two parts (Fig. 13):

- At first the sample was submitted to an asymmetric cyclic loading (OA in Fig. 13a), next two cyclic creep sequences AB and CD are applied, then a second series of cycles EF, and finally two other creep sequences, FG and HI,
- during the second part, a symmetric cyclic loading JK (Fig. 13b) was performed.

The comparison of modes of loading is shown in the Fig. 13c.

The diagrams, shown in Figs. 13a, 13b and 13c, highlight the first order cyclic ratcheting effect during asymmetric cyclic loading for a stress control process. The total shear strain evolution during the test is shown in the Fig. 13d. We can see that the creep sequences (AB, CD, FG and HI) have shapes of creep curves and their unique duration is equal to 900 seconds. The duration of creep sequences is not long enough to reach the saturation stage but we can observe

the existence of two stages: at first (stage I) the shear strain variation is quite fast, and next it is cut down at the end of the creep sequence (stage II).

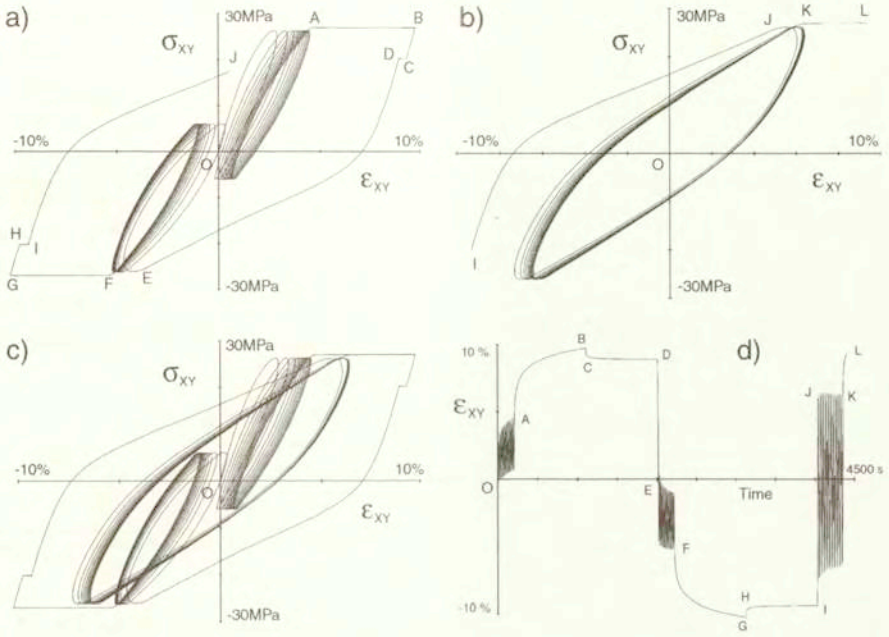

FIG. 13. (a,b,c) cyclic shear at constant intensity of stress rate with creeps, and (d) variations of the shear strain during this test.

These creep effects could be displayed by the variations of the second-order effects (Figs. 14, 15 and 16). Analysing the first part of the cyclic shear test (Fig. 14), we can see that the lateral strain ε^g_{xx} raises during the first sequences of asymmetric cyclic loading (OA in Fig. 14a) and stops during the second one (EF in Fig. 14b). Like in the case of relaxation, we observe a sharp drop in the ratchet intensity during creep sequences AB and CD, but during sequences FG and HI the ratchet intensity drop is negligible. During the second part of the test, when symmetric cyclic loading takes place (JK in Fig. 15a), we notice the return of the ratchet phenomenon. The same is shown in the Fig. 15b as a function of time.

At last, in the Figs. 16a and 16b is shown the evolution of ratchet during the whole cyclic shear at a constant intensity of the stress rate as a function of shear strain and time, respectively.

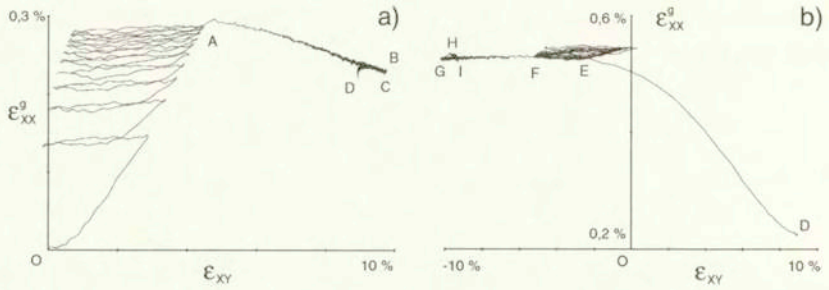

FIG. 14. (a) second-order effect during the OABCD part of the test at the Fig. 13, and (b) during the DEFGHI part of this test.

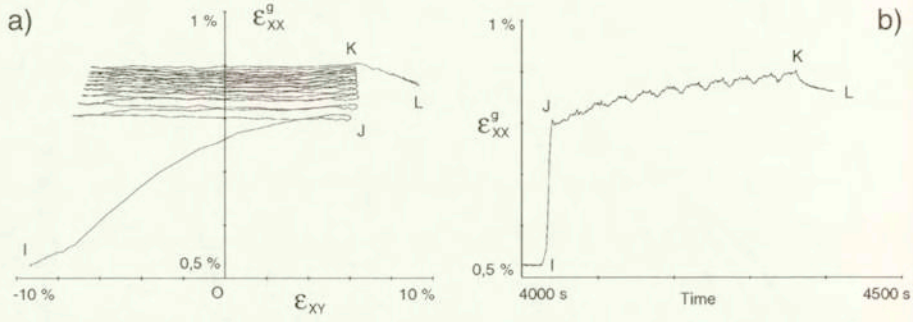

FIG. 15. (a, b) second-order effect during the IJKL part of the test at the Fig. 13.

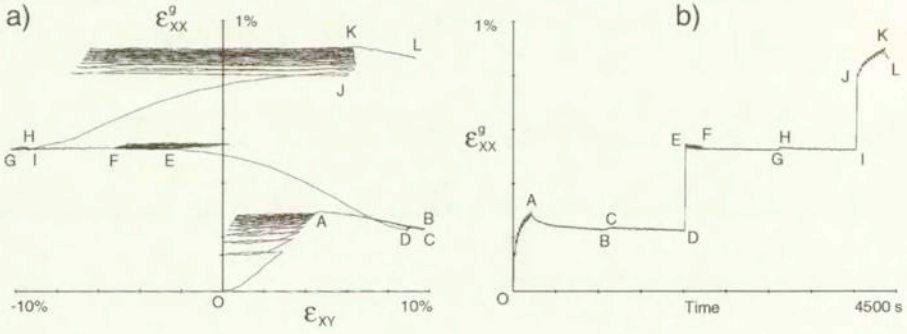

FIG. 16. (a, b) second-order effect during the whole test at the Fig. 13.

3.5. Thermomechanical effects

Comparing mechanical and thermal characteristics obtained during simple shear, we can find the temperature–stress relations $\Delta T(\sigma_{xy})$. Example of this relation is shown in Figs. 17 and 18.

Analysing the obtained results, three stages of deformation – elastic, highly-

elastic and plastic – are noticeable in polyamide PA66 from the thermomechanical coupling point of view:

- In the elastic range of deformation, in agreement with the Kelvin law [15], there are no temperature changes during shearing – the thermoelastic effect is negligibly small.
- During highly-elastic range of deformation, we observe a decrease of temperature; this stage is not observed in metals.
- In the plastic range of deformation, temperature of shear bands always increases.

A thermoelastic effect was not observed during unloading. Temperature decreased as a result of exchange of the heat with metallic grips.

As it was mentioned previously, lateral deformation during cyclic deformation is very small in comparison with the shear strain, then the temperature changes during this process would be similar as during simple shear.

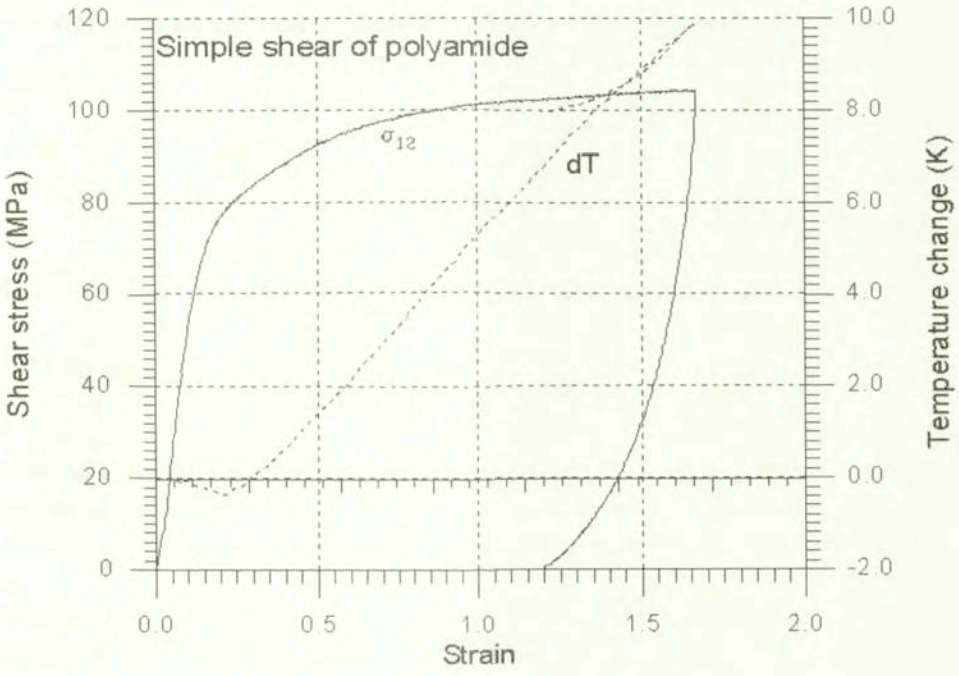

FIG. 17. Stress-strain and temperature-strain relation obtained during simple shear of polyamide.

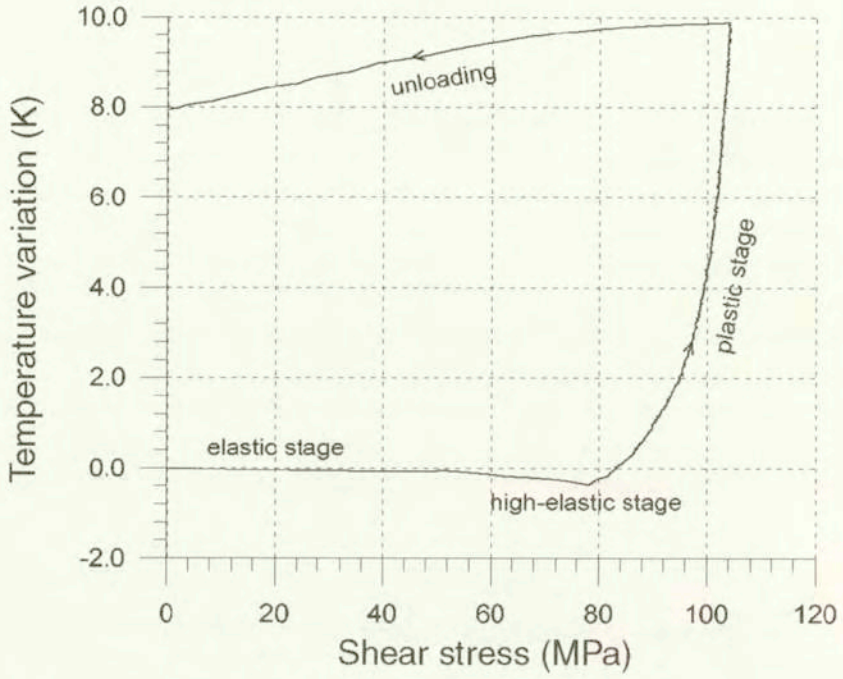

FIG. 18. Thermomechanical effect during simple shear of polyamide.

4. Concluding remarks

Among other conclusions following these shear tests on the PA66 solid polymer, the following phenomena are observed. Firstly, during symmetric cyclic shear tests at constant intensity of strain rate, a transient hardening effect occurs at the first loading, followed by a weak softening with the cyclic path. The limit cycle, reached by softening, is a function of the cycle strain amplitude, independently of the order of the cyclic tests with different amplitudes. The effects of this cyclic softening vanish during a relaxation or a creep sequence. Second-order effects increase the lateral strain ε^g_{xx} during shear without σ_{xx} stress; a ratchet phenomenon occurs during cyclic shear.

In the course of the relaxation sequences, three main stages describe the evolution of the σ_{xy} stress versus the time; the first one is very short and shows quick variations of σ_{xy}, during the second stage the stress evolution is cut down, and the third one is a saturation stage. The ratchet phenomenon on ε^g_{xx} goes back in the opposite direction, during relaxations. According to the comparison of the lateral strain and the shear stress evolution versus the time, the first-order and the second-order effects are very close, during a relaxation sequence.

Finally, investigation of simple shear indicates that the temperature decreases

during the highly-elastic range of deformation. Such phenomenon was not observed in metallic sheets.

With these two series of experiments, we can observe evolution of the shear stress, shear strain and lateral strain when the lateral stress is equal to zero, and the thermomechanical effects in the case of simple shear. Cyclic, relaxation and creep loading were performed. These experimental results give interesting information about the thermomechanical behaviour of the PA66 polyamide in the case of rotational loading of shear.

Acknowledgements

This paper has been partially supported by the Polish Committee for Scientific Research (KBN) under Grant No 8 TO7A0462 : "Thermomechanics of viscoelastoplastic materials subjected to deformation". The first author – G.B., acknowledges the invitation to the Institute of Fundamental Technological Research of PAS, in August-December 2001, in the frame of the Center of Excellence AMAS (Advanced Material and Structures).

References

1. J. H. POYTING, *On pressure perpendicular to the shear planes in finite pure shears, and on the lengthening of loaded wires when twisted*, Proc. Roy. Soc. London, Serie A, **82**, 546-559, 1909.
2. J. H. POYTING, *On the changes in the dimensions of a steel wire when twisted, and on the pressure of distortional waves in steel*, Proc. Roy. Soc. London, Serie A, **86**, 534-561, 1912.
3. A. FOUX, *An experimental investigation of Poynting effect*, Proc. Int. Sym. Second Order Effects Haifa, 228-251, 1962.
4. R. S. RIVLIN, D. W. SAUNDERS, *Large elastic deformations of isotropic materials. VII Experiments on the deformation of rubber*, Phil. Trans. Roy. Soc. London, A 865, **243**, 251-288, 1951.
5. H. W. SWIFT, *Length changes in metals under torsional overstrain*, Engineering, 253-257, April 4, 1947.
6. A. TOURABI, P. GUELIN, D. FAVIER, *Towards the modelling of deformable ferromagnets and ferroelectrics*, Arch. Mech., **47**, 3, 437-483, 1995.
7. P. GUELIN, W. K. NOWACKI, D. QUEREYRON, A. TOURABI, *Ratcheting and constitutive patterns of rate-form defined in Preferred Reference Frames*, Arch. Mech., **51**, 3-4, 357-390, 1999.
8. G. BLES, S. P. GADAJ, P. GUELIN, W. K. NOWACKI, A. TOURABI, *Thermomechanics of viscoplastic large strains of solid polymers*, Arch. Mech, **52**, 3, 397-427, 2000.
9. B. WACK, A. TOURABI, *Cycling shear of metallic sheets: application to aluminium-lithium alloy*, J. Mater. Sci., **28**, 4735-4743, 1993.

10. B. WACK, *The torsion of a tube (or a rod): General cylindrical kinematics and some axial deformation and ratchet measurements*, Acta Mech., **80**, 39, 1989.

11. C. G'SELL, S. BONI, S. SHRIVASTAVA, *Application of the plane simple shear test for determination of the plastic behaviour of solid polymers at large strains*, J. Mater. Sci. Eng. **18**, 903-918, 1983.

12. E. F. RAUCH, J. H. SCHMITT, *Dislocation substructures in mild steel deformed in simple shear*, Mater. Sci. Eng., **A113**, 441-448, 1989.

13. S. P. GADAJ, W. K. NOWACKI, E. A. PIECZYSKA, *Changes of temperatures during the simple shear test of stainless steel*, Arch. Mech., **48**, 4, 779-788, 1996.

14. NGUYEN H. V. W. K. NOWACKI, *Simple shear of metal sheets at high rates of strain*, Arch. Mech., **49**, 2, 369-384, 1997.

15. W. THOMSON,(Lord Kelvin), Quart. J. Pure and Appl. Math, 1, 57, 1857; Math. and Phys. Papers, Cambridge, **1**, 291, 1882.

Received December 19, 2001; revised version February 28, 2002.